

Single RNA Kissing Complexes Studied by Fluorescence Resonance Energy Transfer

Peter B. Yim,^{*} Xiaoyi Zhang,^{*} Eric S. DeJong,[†] J. Meghan Carroll,^{*} John P. Marino,[†]
Lori S. Goldner^{*#}

^{*}Optical Technology Division, National Institute of Standards and Technology, Gaithersburg MD
20899

[†]Center for Advanced Research in Biotechnology, Rockville MD 20850

ABSTRACT

We have used single molecular-pair fluorescence resonance energy transfer (FRET) to probe the conformation of a RNA loop-loop “kissing complex” formed by two small RNA hairpins (R1_{inv} and R2_{inv}) derived from Escherichia coli (*ColE1*) plasmid-encoded transcripts, RNA I and RNA II. This RNA kissing complex is a critical intermediate in a multi-step hybridization pathway which controls plasmid replication.¹ Biotinylated RNA molecules were labeled with donor and acceptor dyes on their 5' ends and immobilized on a biotinylated surface using streptavidin. Fluorescence from the donor and acceptor dyes was collected and measured by photon counting detectors in two spectrally separated channels in a customized confocal microscope. Quantitative measurement of intramolecular distances between 5' ends of the RNA was obtained using donor-only single molecule FRET. This donor-only single molecule FRET technique is described in detail and validated through determination of the distance between 5' ends of 8mer A-form RNA helices of known structure.

Keywords: Single Molecule, FRET, RNA, Confocal microscope, Cy3, Cy5

1. INTRODUCTION

The use of single molecule fluorescence to probe molecular structure and dynamics is providing new insights into how biomolecules function and more recently is being adapted by the biotechnology community for screening and sequencing. Single molecule fluorescence from immobilized fluorophores at room temperature was first detected in 1993;² three years later the first experiment demonstrating fluorescence resonance energy transfer (FRET) from a single molecular-pair³ opened the door to direct observation of such phenomena as metastable states in protein folding,⁴ measurements of the activity of individual enzymes,⁵ and binding and folding of RNA molecules.^{6,7}

Sample-scanning confocal microscopy has become a common method for detecting and measuring single molecules.⁸ In this technique, pinholes are used to spatially filter both excitation and emission light, resulting in excellent background rejection that makes detection of a single fluorophore possible. High quantum-yield single photon counting modules based on avalanche photodiodes (APDs) or photomultiplier tubes (PMTs), and linearized flexure stages that are piezo-electrically driven have made the technique widely available.

In fluorescence resonance energy transfer (FRET), non-radiative energy transfer occurs between an excited dipole (the donor) and another dipole (the acceptor) that has an absorption spectrum that overlaps the emission spectrum of the donor. The probability of energy transfer, also called the FRET efficiency (E), is dependent on the distance between two dipoles, R , and can be expressed as

$$E = \left[1 + \left(\frac{R}{R_0} \right)^6 \right]^{-1} \quad (1)$$

[#] lori.goldner@nist.gov; phone: (301) 975-3792; fax (301) 975-6991

The Förster distance (R_0), for which the probability of energy transfer is 1/2, can be calculated from the spectral properties of the donor and the acceptor.⁹⁻¹¹ Single molecule FRET is typically measured using two spectrally resolved channels, one tuned to the donor emission peak and the other to the acceptor emission peak. We discuss below various techniques for measuring E and metrologic issues that arise in extracting distances from these measurements.

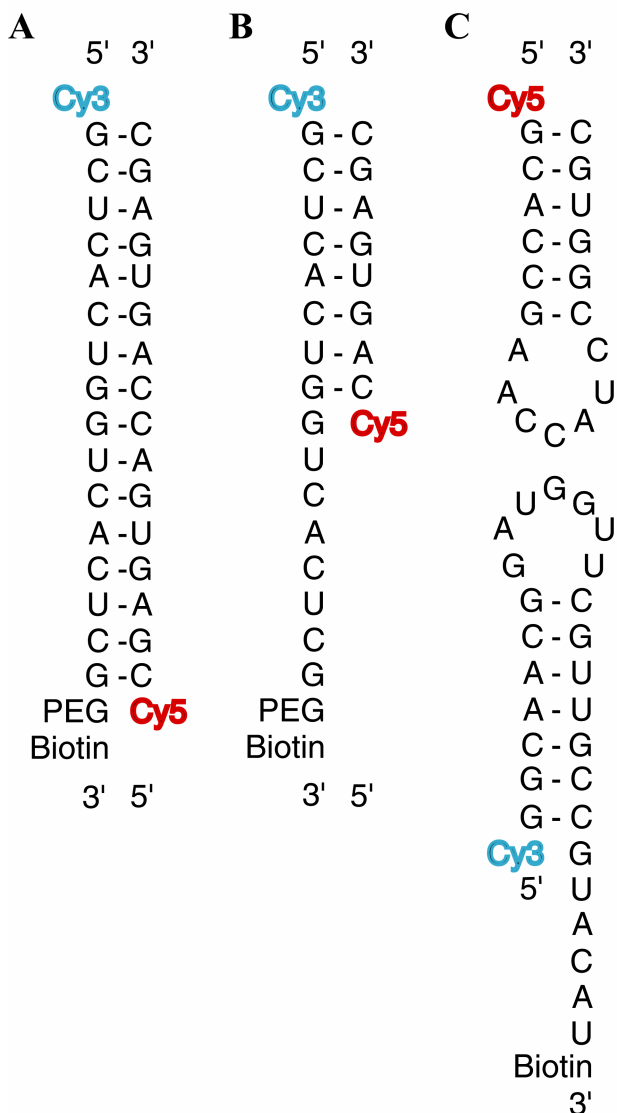


Figure 1. (A) RNA 16mer duplex. Cy dyes were attached to two complementary 16mer strands of RNA using phosphoramidite chemistry. Two hexaethylene glycol molecules were used as a molecular spacer between the Cy3 labeled strand and an attached biotin for surface attachment. (B) RNA 8mer duplex. Cy5 was attached to a RNA 8mer strand using phosphoramidite chemistry, which was designed to be complementary to the first 8 bases in the same Cy3 labeled 16mer strand as shown in (A). (C) R1inv-Cy3 and R2inv-Cy5 of the stem-loop hairpins derived from the *ColE1* plasmid-encoded RNA I and RNA II transcripts. Cy dyes were again linked to 5' end of the RNA strands using phosphoramidite chemistry. In this system, no PEG linker was used to separate the RNA and biotin attached for surface immobilization. Instead, R1inv-Cy3 had unpaired bases that act as a spacer between the RNA and surface. In all systems, biotin formed a linkage between RNA and streptavidin biotinylated-BSA surface.

Here we make single molecular-pair FRET measurements using Cy3 (Indodicarbocyanine-3) as the donor molecule and Cy5 (Indodicarbocyanine-5) as the acceptor molecule. Three separate systems are studied (Fig.1). The first two are double-stranded RNA A-form helices 8 base pairs and 16 base pairs long (Figs. 1A and 1B). For these two molecules, denoted “8mer” and “16mer”, the distance between 5' ends is accurately known and the inter-dye distance can be estimated. The final system is a loop-loop kissing complex formed by two RNA hairpin structures, R1inv and R2inv (Fig. 1C). In *ColE1*, the plasmid-encoded transcript (RNA II) acts as the primer for plasmid replication, while RNA I, a shorter plasmid-encoded transcript, which is antisense to RNA II, acts as the suppressor.^{12,13} RNA I initially binds

RNA II through a loop-loop kissing interaction and isolated stem-loops derived from the RNA transcripts have also been shown to form kissing complexes. Mutant hairpin structures, called R1inv and R2inv, form kissing complexes with enhanced stability.¹ These molecules, shown in Fig. 1C, have been well studied by NMR and have been shown to form Watson-Crick base pairs for all seven complementary loop nucleotides to form a loop-loop helix which is 3' stacked between the two stem helices (Fig. 5).^{1,14} The resulting pseudo-contiguously stacked helical structure is bent towards a compressed major groove of the loop-loop helix.

While the standard NMR methods, which have been used to determine the structure of the R1inv-R2inv kissing complex, provide a highly accurate picture of the local conformation in these complexes, the distance and dihedral restraints obtained using NMR measurements do not allow the long range conformation to be determined with high precision. As a complement to structural restraints determined using NMR methods, single molecule FRET measurements can in principle provide accurate measurement of longer range distances that can be used to determine the global conformation of the RNA. In practice, most studies utilizing single molecular-pair FRET have been qualitative, observing changes in FRET efficiency but not obtaining accurate distance measurements. Here we describe the barriers to quantitative single-pair FRET and show how accurate structural measurements can be achieved.

2. METHODOLOGY

2.1 RNA Synthesis and Purification

R1inv with Cy3 and Biotin, and R2inv with Cy5 (Fig. 1A) were synthetically made on an Applied Biosystem 390 (Perkin-Elmer, Forest City, CA) synthesizer using nucleoside and dye phosphoramidites¹⁵ purchased from Glen Research (Sterling, VA). Tetrabutyl ammonium fluoride removed 2'-hydroxyl silyl protection group of RNA and was dialyzed away with extensive washing with H₂O. The RNA-dye samples were purified with polyacrylamide gel electrophoresis (PAGE) and extracted from the gel by electrophoretic elution. The RNA samples were dialyzed and concentrated using a lyophilizer. The samples were further purified using an Amersham Bioscience size exclusion column (Piscataway, NJ), and RNA concentrations were determined by measuring absorbance at 260 nm.

The RNA 16mer with Cy3 and Biotin, and the RNA 8mer with Cy5 (Figs. 1A and B) were synthesized and purified as described above. The HPLC purified RNA 16mer with Cy5 (Fig. 1A) was ordered from Integrated DNA Technologies (Coralville, IA).

2.2 Confocal Microscopy

The illuminator on a standard inverted fluorescence microscope (Axiovert S100TV, Zeiss, Germany) was removed and the light source replaced with a 532 nm wavelength excitation laser source (Verdi-V10, Coherent, Santa Clara, CA) that was routed through an optical fiber, spatially filtered through a 50 μ m pinhole and expanded to 1.1 cm to overfill the back focal plane of the microscope objective. A 532 nm narrow band pass filter was used after the fiber to reject fiber Raman scattering and a polarizer and a quarter waveplate were used to prepare circularly polarized light. A dichroic mirror (540 DCLP, Omega Optical, Brattleboro, VT) was used to direct excitation light into the objective. The oil immersion objective had numerical aperture 1.3 (Fluar100x, Zeiss, Germany). A piezo driven scanning stage (Physik Instrumente GmbH, Germany) was used to scan the sample, which was prepared on a number 1.5 coverslip surface. Fluorescence was collected through the same objective, and imaged through a 200 μ m pinhole to reject any out of focus fluorescence. A second dichroic mirror (645DCXR, Chroma Technology, Rockingham, VT) was used to separate Cy3 and Cy5 fluorescence. A photon-counting module based on a PMT (Hamamatsu, Bridgewater, NJ) was used for detecting Cy3 emission and a photon-counting module based on an APD (Perkin Elmer, Canada) was used for detecting Cy5 emission. The optics were aligned daily.

2.3 Microscopy Sample Preparation

A simple flow cell was made to introduce samples and measure single molecules. Number 1.5 coverslips (Fisher Scientific, Pittsburgh PA) were soaked in 1 mol/L KOH, methanol, and again in 1 mol/L KOH to clean any chemical residues from the glass. The coverslips were further cleaned in an UV/ozone chamber. A flow cell was made between two cleaned coverslips using 170 μ m thick glass spacers and silicone vacuum grease. To create a biotinylated surface, 100 μ L of 1 mg/ml biotinylated BSA (Sigma, St. Louis MO) in Tris buffer consisting of 20 mmol/L Tris-HCl (nominal

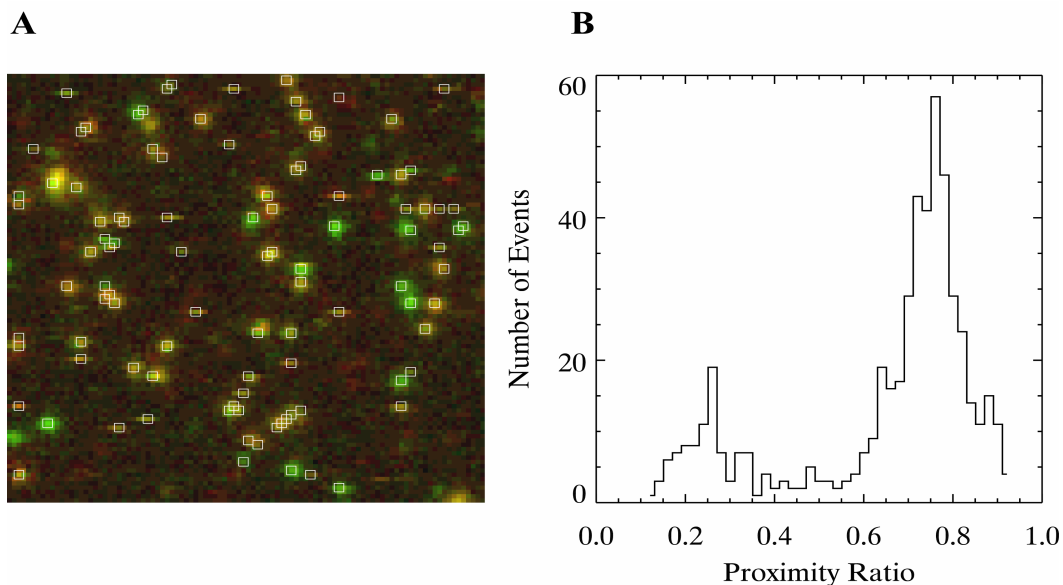


Figure 2. (A) A two-channel image of surface-tethered RNA 16mer duplex. Here green indicates donor fluorescence [0 counts – 216 counts], red indicates acceptor fluorescence [0 counts – 481 counts]. The acceptor channel has a 6.3 count average background, and the donor channel has a 1.3 count average background. The sampling time at each pixel in this 100 pixel square image was 5 ms and the excitation power was nominally 11 kW/cm². This image is 10 μm \times 10 μm . (B) A histogram of proximity ratios from the image. Ratios are calculated in a 3 pixel by 3 pixel square centered around local fluorescence maxima. The squares indicate the region around each maxima from which ratios were calculated. Only pixels from these regions, and with 60 or more total counts, are used in the histogram and the background has been subtracted. The peak near $P = 0.75$ contains the data for which FRET occurs; the peak near $P = 0.25$ contains molecules for which the acceptor has bleached; this peak gives us the crosstalk into the donor channel.

pH 7.2) and 50 mmol/L NaCl was introduced. The surface was rinsed with 200 μL of Tris buffer after 10 minutes incubation. Streptavidin (100 μL of 0.2 mg/ml) in Tris buffer was then introduced to bind with biotin. After 10 minutes incubation, the excess streptavidin was washed away with Tris buffer. Biotinylated RNA sample was then added and formed biotin-streptavidin linkages to the surface.

R1inv-Cy3 and R2inv-Cy5 were stored in 10 $\mu\text{mol/L}$ stock solution. They were incubated at $T > 85$ $^{\circ}\text{C}$ for 3 minutes and snap cooled in dry ice for 3 minutes to ensure hairpin structures. All the RNA samples were hybridized at concentration ≥ 0.2 $\mu\text{mol/L}$ and diluted immediately before the experiments. R1inv and R2inv samples were incubated in the presence of Tris buffer plus 5 mmol/L MgCl₂ to form a kissing complex. After successive initial measurements, it was determined that a concentration of 50 pmol/L RNA gave good surface density and this concentration was used in subsequent measurements. Free RNA was removed from the flow cell by rinsing with the oxygen scavenger buffer (Tris buffer with addition of β -D-glucose at 10% mass fraction, 2-mercaptoethanol at 1% volume fraction, 0.1 mg/ml glucose oxidase [Roche Applied Science, Indianapolis IN], and 0.02 mg/ml catalase [Roche Applied Science, Indianapolis IN]). The measurements were done with the sample in this buffer.

2.4 Data Acquisition

The output of the photon-counting detectors was recorded using data acquisition boards (National Instruments PCI-6602, Austin TX) and LabView (also National Instruments). The scanning rate for data collection was typically 5 ms per pixel, and the bin time for intensity vs. time data was also typically 5 ms. The data were analyzed using our own software written in IDL (Research Systems Inc., Boulder CO).

A typical image acquired for a 16mer sample is shown in Fig. 2A. Donor and acceptor channel images are overlaid, with the donor channel marked with symbols and points and the acceptor channel with a line. The background,

measured in a “dark” region of the image, is 1.3 counts in 5 ms (*e.g.*, 260 Hz count rate) in the donor channel (PMT detector) and 6.3 counts in 5 ms (*e.g.*, 1260 Hz count rate) in the acceptor channel (APD detector).

A typical FRET trajectory for the 8mer sample is shown in Fig. 3A. The data were acquired in 5 ms bins but are displayed in 50 ms bins. Donor data are shown as points or symbols and acceptor data are a line. At just over 15 s the acceptor photobleaches and the donor signal increases. Due to crosstalk from the donor into the acceptor channel, the signal in the acceptor channel is not equal to the background signal after the acceptor photobleaches. After 25 s the donor photobleaches (not shown) and the background signal for both channels can be measured. In general we used data where only these two photobleaching events were present and where the acceptor bleached first, permitting a measurement of the crosstalk. Crosstalk from the acceptor into the donor channel is negligible.

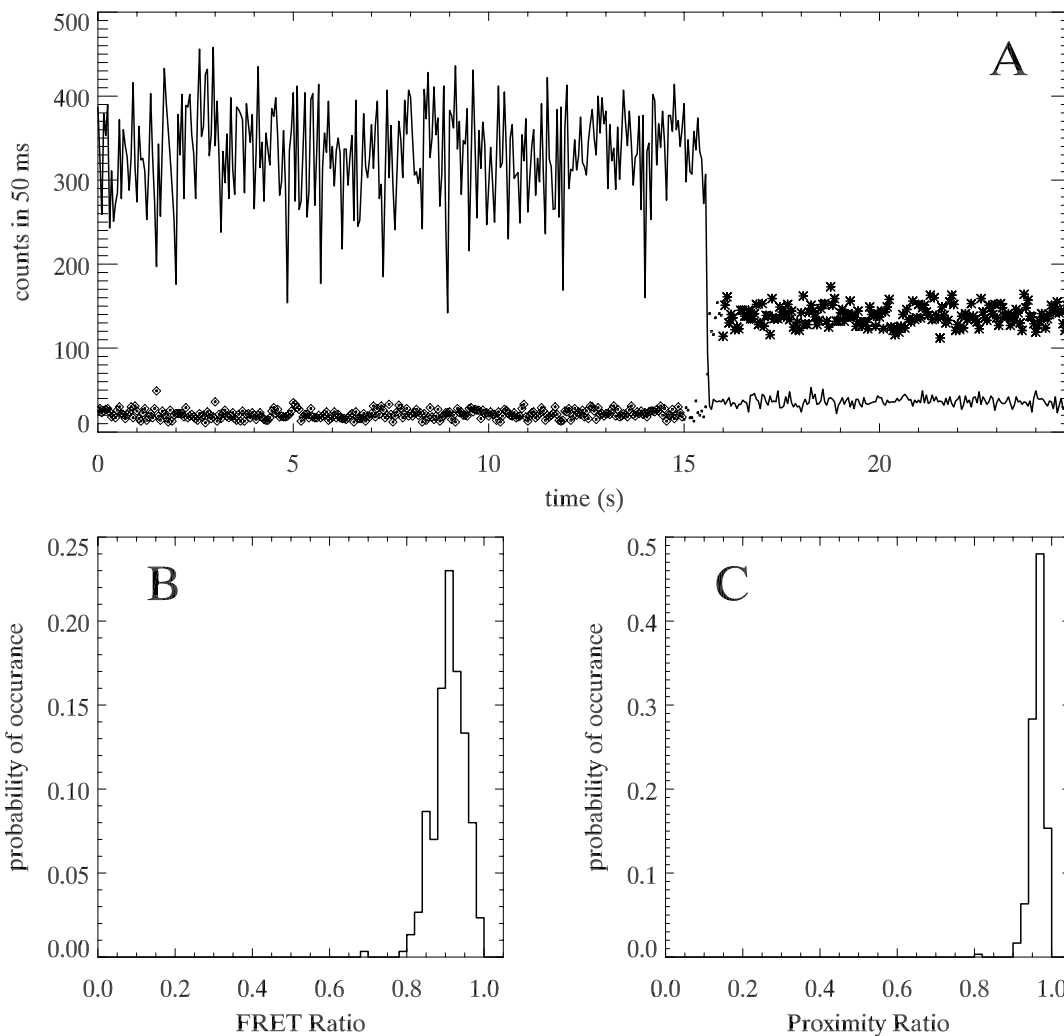


Figure 3. (A) Intensity vs. time trajectory of a single RNA 8mer duplex on the surface. The points are the signal in the acceptor (Cy5) channel and the line is the signal in the donor (Cy3) channel. (B) Histogram of FRET values calculated using Eq. (13) and the data marked with \diamond . Data marked with * were used to determine the average value of the donor fluorescence after acceptor bleaching. (C) Histogram of proximity ratio values calculated using Eq. (11) and the data for which the donor channel is marked with \diamond .

2.5 Analysis

The analysis of FRET data has been discussed by others, in the context of both bulk^{10,16} and single molecule measurements.¹⁷ Here we elucidate the features of this analysis that are relevant to our work and discuss how quantitative FRET data, which are difficult to obtain in bulk systems, can be obtained for single-pair FRET.

In the analysis below we will need to know the fluorescence intensity from the donor and acceptor dyes. If we call the measured signals in the donor and acceptor channels S_D and S_A , then the relationship between S_D and S_A and the donor and acceptor count-rates, I^D and I^A , is:

$$S_D = X_{DD}I^D + B_D \quad (2)$$

$$S_A = X_{AA}I^A + X_{AD}I^D + B_A \quad (3)$$

Here, B_D (B_A) is the background into the donor (acceptor) channel; X_{AA} (X_{DD}) is the collection efficiency of the acceptor (donor) channel (includes for example the detector, filters, and lens efficiency); and X_{AD} is the efficiency with which the donor molecule fluorescence is detected in the acceptor channel (the crosstalk). It is assumed here that the efficiency with which acceptor fluorescence is detected in the donor channel is negligible. We can measure the background after both molecules have photobleached (then $S_D = B_D$ and $S_A = B_A$, and we can measure the ratio of the crosstalk to the donor-channel collection efficiency when an acceptor molecule photobleaches but the donor has not. In this case, setting $I^A = 0$ in Eq. (3) and dividing Eq. (3) by Eq. (2) we find:

$$\frac{X_{AD}}{X_{DD}} = \frac{S_A - B_A}{S_D - B_D} = \frac{S'_A}{S'_D} \quad (4)$$

where $S'_A \equiv S_A - B_A$ and $S'_D \equiv S_D - B_D$. Solving Eq. (2) for I^D we find:

$$I^D = \frac{S'_D}{X_{DD}} \quad (5)$$

and using this expression for I^D in Eq. (3) we solve for I^A :

$$I^A = \frac{S'_A}{X_{AA}} - \frac{X_{AD}}{X_{AA}} \frac{S'_D}{X_{DD}} \quad (6)$$

When the quantum yields and extinction ratios of the dyes are unaffected by the presence of the energy transfer partner, the expressions for the total fluorescence from the donor, I^D , and the acceptor, I^A , are given by:¹⁰

$$I^D = (1-E)\varepsilon^D(\nu_0)\Phi^D(\Delta\nu_D) \quad (7)$$

$$I^A = E\varepsilon^D(\nu_0)\Phi^A(\Delta\nu_A) + \varepsilon^A(\nu_0)\Phi^A(\Delta\nu_A) \quad (8)$$

where E is the probability of energy transfer (FRET efficiency); $\Phi^A(\Delta\nu_A)$ and $\Phi^D(\Delta\nu_D)$ are the quantum yields of the acceptor and donor, respectively, over the band of wavelengths $\Delta\nu_A$ and $\Delta\nu_D$ determined by our filter sets; and $\varepsilon^D(\nu_0)$ and $\varepsilon^A(\nu_0)$ are the extinction ratios of the donor and acceptor, respectively, at the excitation wavelength, ν_0 . If and only if the direct excitation of the acceptor is negligible, we can set the second term on the right side of Eq. (8) equal to zero and solve for E in terms of the quantum yields eliminating the donor extinction ratio using Eq. (7):

$$E = \frac{I^A}{I^A + \left(\frac{\Phi^A}{\Phi^D}\right)I^D} \quad (9)$$

If we substitute into this equation the expressions for I^D and I^A from Eqs. (5) and (6), we see that:

$$E = \frac{S'_A - \frac{X_{AD}}{X_{DD}}S'_D}{S'_A - \frac{X_{AD}}{X_{DD}}S'_D + \left(\frac{\Phi^A}{\Phi^D}\right)\frac{X_{AA}}{X_{DD}}S'_D} \quad (10)$$

Unfortunately it is not generally the case that the direct excitation of the acceptor is negligible. It can also be difficult or impossible to discern the relative quantum yields of the dyes, or the ratio of the collection efficiencies between the

donor and acceptor channels. In most single molecule literature, the ratio $\left(\frac{\Phi^A}{\Phi^D}\right)\frac{X_{AA}}{X_{DD}}$ is set equal to 1 and the resulting expression is referred to as the proximity ratio, P :

$$P = \frac{S'_A - \frac{X_{AD}}{X_{DD}} S'_D}{S'_A - \frac{X_{AD}}{X_{DD}} S'_D + S'_D} \quad (11)$$

In many cases the crosstalk is assumed or measured to be negligible and then this is further simplified to $P = \frac{S'_A}{S'_A + S'_D}$.¹⁸ It should be noted that R , the distance between the dyes, cannot be extracted from P . However, since our single molecule trajectories generally show the acceptor bleaching first, we can use an expression for E based only the donor fluorescence. In this case we note that after the acceptor bleaches we can write:

$$I_{noA}^D = \epsilon^D (v_0) \Phi^D (\Delta V) \quad (12)$$

and then from Eqs. (7) and (12) we see that

$$E = 1 - \frac{I^D}{I_{noA}^D} = 1 - \frac{S'_D}{S'_{DnoA}} \quad (13)$$

This will be correct so long as the quantum yield, and extinction ratio, and spectrum of the donor is not affected by the fact that the acceptor is photobleached. There is no dependence on the quantum yields or collection efficiency of the microscope, no difficulty if there is direct excitation of the acceptor, and this expression for E can be used with Eq. (1) to determine R .

3. RESULTS

Figures 3 and 4 demonstrate FRET and proximity ratio measurements on an 8mer and an R1inv-R2inv kissing complex. The value for S'_{DnoA} is calculated by averaging the data points, taken after the acceptor bleaches, that are marked with * and subtracting the average background value after both donor and acceptor have photobleached. A correct value for S'_{DnoA} can be difficult to discern and uncertainties are also hard to determine, since triplet blinking and other photophysical phenomena result in non-Poissonian statistics. For the 8mer data shown in Fig. 3, $\langle S'_{DnoA} \rangle = 12.86 \pm 0.08$ counts in 5 ms bins, and the donor background was 0.97 counts in 5 ms bins (the acceptor background was 1.58 counts in 5 ms bins). For the uncertainty on the mean we assume a Poisson distribution and use the usual formula for the standard deviation of the mean; to the extent that these distributions are non-Poissonian we are underestimating this uncertainty. We note that for these data, $\langle S_{DnoA} \rangle = 13.83$ counts and the rms of the distribution is 3.84 counts, which is slightly higher than the shot noise value of 3.72 counts. Before photobleaching occurs, we use the points marked with \diamond to calculate $\langle S'_D \rangle = 1.16 \pm 0.02$. From Eq. (13), $\langle E \rangle = 0.910 \pm 0.002$.

For the R1inv-R2inv data shown in Fig. 4, the mean value of $\langle S'_{DnoA} \rangle = 23.7 \pm 0.1$ counts in 5 ms bins, while $\langle S'_D \rangle = 14.7 \pm 0.1$, giving $\langle E \rangle = 0.378 \pm 0.004$. The donor background is 2.2 counts and the acceptor background is 3.2 counts. Here the distribution is farther from Poissonian; $\langle S_{DnoA} \rangle = 25.9$ counts with an rms spread of 5.9 counts, compared to 5.1 counts expected in the Poisson limit.

FRET histograms are shown in Figs. 3B and 4B. Here a histogram is calculated from the values $E = 1 - \frac{S'_D}{\langle S'_{DnoA} \rangle}$, where

the S'_D are again given by the data marked with \diamond . We expect for these systems that there should be only one stable configuration of the molecule, and so we expect to see only a single peak on the FRET histogram. The average values for FRET calculated above assume a single molecular configuration, and indeed only one peak is visible in the histograms. The values for E are reproducible over months during which data were taken, although the spread in the

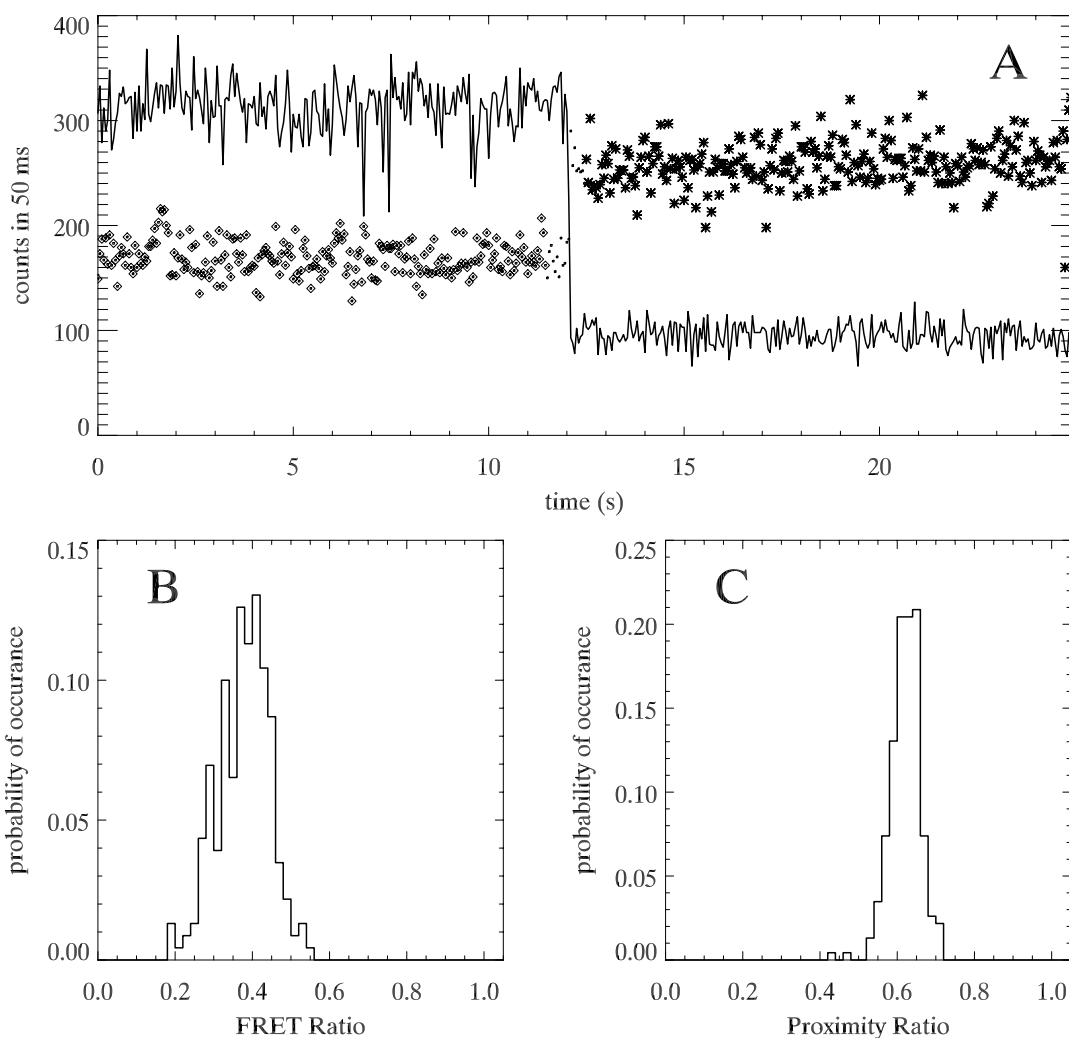


Figure 4. (A) Intensity vs. time trajectory of a single R1inv-R2inv kissing complex on the surface. The line is the signal in the acceptor (Cy5) channel and the points are signal in the donor (Cy3) channel. (B) Histogram of FRET values calculated using Eq. (13) and the data marked with \diamond . Data marked with * were used to determine the average value of the donor fluorescence after acceptor bleaching. (C) Histogram of proximity ratio values calculated using Eq. (11) and the data for which the donor channel is marked with \diamond .

accumulated distribution is larger than expected, which might be attributed to the non-Poissonian nature of single molecule fluorescence, or to conformational flexibility.

Proximity ratio histograms are shown in Figs. 3C and 4C. Here the crosstalk $\frac{X_{AD}}{X_{DD}}$ is determined using Eq. (4) and the data for which the donor points are marked with *, since for these data the acceptor has photobleached and any remaining acceptor signal is due to crosstalk and background. The proximity ratio is calculated using Eq. (11) from the data points where the donor values have been marked with \diamond . Background is measured after both dyes have photobleached, exactly as for the FRET determinations. Even for freely-rotating dyes, the average value of the proximity ratio varies significantly from day to day and even hour to hour as the focus, microscope alignment, or PMT efficiency changes. We believe a main contributor to drift is temperature change; as the temperature drifts, the focus of the microscope drifts and chromatic aberrations cause the coupling through the confocal pinhole to change.

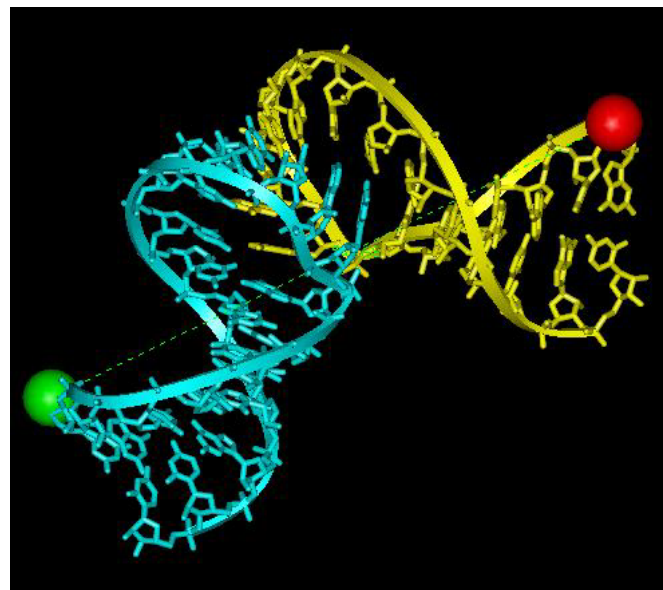


Figure 5. Ribbon and stick representation of the average, minimized NMR-determined structure¹ of the R1inv-R2inv kissing complex. R1inv sequence is in blue color with the phosphate backbone shown as a ribbon, bases shown as sticks, and a Cy3 dye shown as green ball. R2inv sequence is in yellow color with the phosphate backbone shown as a ribbon, bases shown as sticks, and a Cy5 dye shown as red ball. The dotted line between two balls was drawn to represent the distance between two dyes.

The width of the proximity ratio distribution is narrower than the width of the FRET ratio distribution; this is because in the measurement of proximity ratio, any fluctuations in the intensity of the donor molecule (*e.g.* due to triplet shelving, conformational changes of the molecule or changes in the local environment unrelated to FRET) are, for the most part, removed by taking the ratio of the intensities. In the donor only measurements, these fluctuations are indistinguishable from changes in the FRET measurement and so the distribution is broader, and (more troubling) possibly shifted from its correct value. The proximity ratio measurement has better precision but, because of the large uncertainty in $\left(\frac{\Phi^A}{\Phi^D}\right)\frac{X_{AA}}{X_{DD}}$, considerably worse accuracy than the donor-only measurement when used to determine inter-dye distances.

4. DISCUSSION

The Förster distance $R_0 = \left[(8.79 \times 10^{-28}) n^{-4} \kappa^2 \Phi^D J \right]^{1/6}$, where J is a spectral overlap integral,^{10,19} was calculated from the measured emission spectrum of RNA 16mer-Cy3 hybridized with an unlabeled complementary RNA 16mer and the measured absorption spectrum of RNA 8mer-Cy5. Here Φ^D is the quantum yield of the donor, n is the refractive index of water and $\kappa = \hat{\mu}_D \cdot \hat{\mu}_A - 3(\hat{\mu}_D \cdot \hat{R})(\hat{\mu}_A \cdot \hat{R})$ is an orientation factor.¹⁰ It is generally assumed that the dyes in a FRET experiment will be freely rotating, so that the average value $\kappa^2 = 2/3$ can be used. Assuming the dyes freely rotate, we find $R_0 = 5.8$ nm for the Cy3 and Cy5 pair, which is within the published range of 5.0 nm to 6.5 nm.²⁰⁻²⁴

For the 8mer RNA data of Fig. 3, Eq. (1) and the measured value for E reported above gives $R = 3.9$ nm \pm 0.1 nm, if $R_0 = 5.8$ nm. However, there is significant evidence that the cyanine dyes are not freely rotating while attached to RNA or DNA and in fact they base stack and are fixed on the ends of the RNA.²³

We can use the base stacking of the cyanine dyes to our advantage. For base-stacked dyes, and using Ref. 23 for the dye coordinates, we predict that the RNA 8mer duplex will have an inter-dye distance of $R = 2.96$ nm and $\kappa^2 = 0.0636$. The R value 3.9 nm reported above is clearly too high in comparison to 2.96 nm, which is understandable given our original assumption that $\kappa^2 = 2/3$. Using Eq. (1) with the measured E and modeled R , we can predict $R_0 = 4.35$ nm \pm 0.02 nm. Given $\kappa^2 = 0.0636$, we can calculate $R_0^6 / \kappa^2 = 106900 \pm 2900$, which for freely-rotating dyes results in $R_0 = 6.4$ nm. A more global attempt to determine R_0^6 / κ^2 and account for the variation between individual molecules from surface effects or conformational flexibility will be the subject of future work.

A stick representation of the average conformation of R1inv-R2inv calculated from an ensemble of eight minimum energy NMR structures¹ is shown in Fig. 5. Using the average R1inv-R2inv structure and modeling the attached Cy dyes as stacked at the end each stem helix, the inter-dye distance is found to be $R = 5.69$ nm and $\kappa^2 = 0.259$. Using these results for R and κ^2 , and using $R_0^6 / \kappa^2 = 106900 \pm 2900$, we can predict using Eq. (1) that $\langle E \rangle = 0.457 \pm 0.006$. Comparison with the measured value $\langle E \rangle = 0.378 \pm 0.004$ shows a clear disagreement; but note that if κ^2 does not change, a distance change of only 0.3 nm, to $R = 6.00$ nm, is sufficient to account for this difference in $\langle E \rangle$. With our current measurement accuracy, we should be able to distinguish between the various minimum-energy conformations of the R1inv-R2inv system; this is the subject of current work in our laboratory.

There are still unresolved difficulties in the use of Cy3 and Cy5 for our FRET pair. Cy5 in particular undergoes frequent long-lived (seconds) transitions to what appears to be a “dark” state, in which it neither accepts energy from the donor nor does it fluoresce from direct excitation. In effect, Cy5 “turns off.” We see this behavior in roughly half of the 16mer and R1inv-R2inv molecules that we study. Short lived conformational transitions of Cy5²⁵ might explain this effect. “Dark” Cy5 is also known to quench Cy3 when the two dyes are in close proximity;²⁶ the inter-dye distances in our case should preclude this possibility, but certainly such an effect would be problematic in our attempt to distinguish different minimum-energy structures.

In this work we have discussed donor-only FRET measurements, which provide accuracy in the measurement of the FRET efficiency at the expense of precision. An accurate determination of $\left(\frac{\Phi^A}{\Phi^D}\right) \frac{X_{AA}}{X_{DD}}$ would permit us to use Eq. (10) to obtain FRET values and therefore increase the precision of our measurement. Global calibration of $\left(\frac{\Phi^A}{\Phi^D}\right) \frac{X_{AA}}{X_{DD}}$ can be difficult because the collection efficiencies of the microscope drift with time and vary with the orientation of the dye emission-dipoles. However, we can use the donor-only technique to effectively calibrate $\left(\frac{\Phi^A}{\Phi^D}\right) \frac{X_{AA}}{X_{DD}}$ for each individual molecule by setting the average value of E obtained from Eq. (10) to the average value of E obtained from the donor-only measurement [Eq. (13)]. In the absence of direct excitation of the acceptor, this procedure permits us to evaluate FRET with the accuracy of the donor-only measurement and the precision of the ratiometric (proximity ratio) method.

ACKNOWLEDGMENTS

This work was funded through the NIST competence program. Note, certain commercial equipment, instruments, or materials are identified in this paper to foster understanding. Such identification does not imply recommendation or endorsement by the National Institute of Standards and Technology, nor does it imply that the materials or equipment identified are necessarily the best available for the purpose.

REFERENCES

- 1 J. P. Marino, R. S. Gregorian, G. Csankovszki, and D. M. Crothers, “Bent helix formation between RNA hairpins with complementary loops,” *Science* **268**, 1448-1454 (1995).
- 2 E. Betzig and R. J. Chichester, “Single molecules observed by near-field scanning optical microscopy,” *Science* **262**, 1422-1425 (1993).
- 3 T. Ha, T. Enderle, D. F. Ogletree, D. S. Chemla, P. R. Selvin, and S. Weiss, “Probing the interaction between two single molecules: fluorescence resonance energy transfer between a single donor and a single acceptor,” *Proceedings of the National Academy of Sciences of the United States of America* **93**, 6264-6268 (1996).
- 4 E. A. Lipman, B. Schuler, O. Bakajin, and W. A. Eaton, “Single-molecule measurement of protein folding kinetics,” *Science* **301**, 1233-1235 (2003).
- 5 H. P. Lu, L. Y. Xun, and X. S. Xie, “Single-molecule enzymatic dynamics,” *Science* **282**, 1877-1882 (1998).
- 6 T. Ha, X. W. Zhuang, H. D. Kim, J. W. Orr, J. R. Williamson, and S. Chu, “Ligand-induced conformational changes observed in single RNA molecules,” *Proceedings of the National Academy of Sciences of the United States of America* **96**, 9077-9082 (1999).

- 7 X. W. Zhuang, L. E. Bartley, H. P. Babcock, R. Russell, T. J. Ha, D. Herschlag, and S. Chu, "A single-molecule study of RNA catalysis and folding," *Science* **288**, 2048-2051 (2000).
- 8 J. J. Macklin, J. K. Trautman, T. D. Harris, and L. E. Brus, "Imaging and time-resolved spectroscopy of single molecules at an interface," *Science* **272**, 255-258 (1996).
- 9 T. Forster, "Energiewanderung und fluoreszenz," *Naturwissenschaften* **6**, 166-175 (1946).
- 10 R. M. Clegg, "Fluorescence resonance energy transfer and nucleic acids," *Methods in Enzymology* **211**, 353-388 (1992).
- 11 L. Stryer and R. P. Haugland, "Energy transfer: a spectroscopic ruler," *Proceedings of the National Academy of Sciences of the United States of America* **58**, 719-726 (1967).
- 12 Y. Eguchi and J. Tomizawa, "Complex formed by complementary RNA stem-loops and its stabilization by a protein - function of *ColE1* ROM protein," *Cell* **60**, 199-209 (1990).
- 13 Y. Eguchi and J. Tomizawa, "Complexes formed by complementary RNA stem-loops - their formations, structures and interaction with *ColE1* ROM protein," *Journal of Molecular Biology* **220**, 831-842 (1991).
- 14 A. J. Lee and D. M. Crothers, "The solution structure of an RNA loop-loop complex: the *ColE1* inverted loop sequence," *Structure* **6**, 993-1005 (1998).
- 15 S. L. Beaucage and M. H. Caruthers, "Deoxynucleoside phosphoramidites - a new class of key intermediates for deoxypolynucleotide synthesis," *Tetrahedron Letters* **22**, 1859-1862 (1981).
- 16 R. M. Clegg, in *Fluorescence Imaging Spectroscopy and Microscopy; Vol. 137*, edited by X. F. Wang and B. Herman (John Wiley & Sons, Inc., 1996).
- 17 T. J. Ha, A. Y. Ting, J. Liang, W. B. Caldwell, A. A. Deniz, D. S. Chemla, P. G. Schultz, and S. Weiss, "Single-molecule fluorescence spectroscopy of enzyme conformational dynamics and cleavage mechanism," *Proceedings of the National Academy of Sciences of the United States of America* **96**, 893-898 (1999).
- 18 T. Ha, "Single-molecule fluorescence resonance energy transfer," *Methods* **25**, 78-86 (2001).
- 19 T. Forster, in *Modern Quantum Chemistry*, edited by O. Sinanoglu (Academic, New York, 1965), p. 93-160.
- 20 R. Yasuda, T. Masaïke, K. Adachi, H. Noji, H. Itoh, and K. Kinoshita, "The ATP-waiting conformation of rotating F-1-ATPase revealed by single-pair fluorescence resonance energy transfer," *Proceedings of the National Academy of Sciences of the United States of America* **100**, 9314-9318 (2003).
- 21 M. C. Murphy, I. Rasnik, W. Cheng, T. M. Lohman, and T. J. Ha, "Probing single-stranded DNA conformational flexibility using fluorescence spectroscopy," *Biophysical Journal* **86**, 2530-2537 (2004).
- 22 I. Rasnik, S. Myong, W. Cheng, T. M. Lohman, and T. Ha, "DNA-binding orientation and domain conformation of the *E-coli* Rep helicase monomer bound to a partial duplex junction: single-molecule studies of fluorescently labeled enzymes," *Journal of Molecular Biology* **336**, 395-408 (2004).
- 23 D. G. Norman, R. J. Grainger, D. Uhrin, and D. M. J. Lilley, "Location of cyanine-3 on double-stranded DNA: Importance for fluorescence resonance energy transfer studies," *Biochemistry* **39**, 6317-6324 (2000).
- 24 S. C. Blanchard, H. D. Kim, R. L. Gonzalez, J. D. Puglisi, and S. Chu, "tRNA dynamics on the ribosome during translation," *Proceedings of the National Academy of Sciences of the United States of America* **101**, 12893-12898 (2004).
- 25 J. Widengren and P. Schwille, "Characterization of photoinduced isomerization and back-isomerization of the cyanine dye Cy5 by fluorescence correlation spectroscopy," *Journal of Physical Chemistry A* **104**, 6416-6428 (2000).
- 26 T. Ha and J. Xu, "Photodestruction intermediates probed by an adjacent reporter molecule," *Physical Review Letters* **90**, 223002 (2003).